Liquid Crystals
Publication details, including instructions for authors and subscription information:
http://www.informaworld.com/smpp/title~content=t713926090

Dielectric relaxation studies and electro-optical measurements in poly(triethylene glycol dimethacrylate)/nematic E7 composites exhibiting an anchoring breaking transition

A. R. E. Brás[a]; O. García[b]; M. T. Viciosa[a]; S. Martins[a]; R. Sastre[b]; C. J. Dias[c]; J. L. Figueirinhas[de]; M. Dionísio[a]
[a] REQUIMTE, Departamento de Química, Faculdade de Ciências e Tecnologia da Universidade Nova de Lisboa, 2829-516 Caparica, Portugal [b] Instituto de Ciencia y Tecnología de Polímeros (C.S.I.C.) - C/Juan de la Cierva, 3, 28006-Madrid, Spain [c] Departamento de Ciências dos Materiais - CENIMAT, Faculdade de Ciências e Tecnologia da Universidade Nova de Lisboa, 2829-516 Caparica, Portugal [d] Centro de Física da Matéria Condensada, Universidade de Lisboa, 2P-1649-003 Lisboa, Portugal [e] Instituto Superior Técnico, 1049-001 Lisboa, Portugal

To cite this Article Brás, A. R. E. , García, O. , Viciosa, M. T. , Martins, S. , Sastre, R. , Dias, C. J. , Figueirinhas, J. L. and Dionísio, M.(2008) 'Dielectric relaxation studies and electro-optical measurements in poly(triethylene glycol dimethacrylate)/nematic E7 composites exhibiting an anchoring breaking transition', Liquid Crystals, 35: 4, 429 — 441
To link to this Article: DOI: 10.1080/02678290801932850
URL: http://dx.doi.org/10.1080/02678290801932850

Liquid Crystals,
Vol. 35, No. 4, April 2008, 429–441

Taylor & Francis
Taylor & Francis Group

Dielectric relaxation studies and electro-optical measurements in poly(triethylene glycol dimethacrylate)/nematic E7 composites exhibiting an anchoring breaking transition

A. R. E. Brás[a], O. García[d], M. T. Viciosa[a], S. Martins[a], R. Sastre[d], C. J. Dias[b], J. L. Figueirinhas[ce] and M. Dionísio[a]*

[a]*REQUIMTE, Departamento de Química, Faculdade de Ciências e Tecnologia da Universidade Nova de Lisboa, 2829-516 Caparica, Portugal;* [b]*Departamento de Ciências dos Materiais - CENIMAT, Faculdade de Ciências e Tecnologia da Universidade Nova de Lisboa, 2829-516 Caparica, Portugal;* [c]*Centro de Física da Matéria Condensada, Universidade de Lisboa, Av. Prof. Gama Pinto, 2P-1649-003 Lisboa, Portugal;* [d]*Instituto de Ciencia y Tecnología de Polímeros (C.S.I.C.) – C/Juan de la Cierva, 3, 28006-Madrid, Spain;* [e]*Instituto Superior Técnico, Av. Rovisco Pais, 1049-001 Lisboa, Portugal*

(Received 29 August 2007; final form 21 January 2008)

Electric field driven anchoring breakage in poly(triethylene glycol dimethacrylate)/nematic E7 composites was studied using dielectric spectroscopy and transmittance measurements. The transmittance hysteresis observed on increasing and decreasing an applied electric field, associated with different alignment states of the liquid crystal (LC), was monitored through dielectric loss. Essential changes are felt mainly in the δ-peak, i.e. the dielectric response of the nematic when the director lies parallel to the applied electric field. An irreversible effect persists after the field had exceeded a critical value, which was manifest in a higher transmittance and a higher dielectric strength of the δ-peak in the OFF state. The initial scattering/opaque state of the sample can only be recovered by heating to the clearing temperature of the nematic LC. The effect referred, commonly called memory effect, is rationalized in terms of anchoring breakage of the LC at the polymer–LC interfaces. The electro-optical response was tested for different poly(triethylene glycol dimethacrylate)/nematic E7 composites in different composition ratios prepared by polymerisation-induced phase separation. The lowest threshold field was observed for the 30:70 composite.

Keywords: PDLC; electro-optical response; dielectric relaxation; anchoring transition

1. Introduction

Polymer–liquid crystal composites have been studied for quite some time in view of their relevance both technologically and in fundamental physics (*1–6*). Among these composites, polymer-dispersed liquid crystals (PDLCs) have received the widest attention (*1, 2*). PDLCs are generally formed by nematic LC droplets dispersed in a polymer host capable of being switched electrically from an opaque scattering state to a highly transparent state. PDLCs with low polymer content give rise to interconnected LC structures and exhibit similar electro-optical behaviours. Opacity is due to a dispersion of the incident light since the principal optical axes of the droplets or LC-rich inclusions are randomly oriented in the polymer host (*7*). The application of the electric field reorients the nematic director, changing the effective LC refractive index. Transparency is achieved when the refractive index of the LC domains match that of the polymer matrix.

It is known that a nematic fluid in contact with a solid substrate adopts a preferred alignment referred to as anchoring, which is dominated by the microscopic interactions at the interfaces between the LC and the polymer matrix (*8*) and plays a major role in the driving voltage of a PDLC. The electric field performs work on aligning the director, increasing the elastic deformation free energy in moving from an orientation largely imposed by the polymer wall to the high-field orientation (*5*). After the electric field is removed, elastic forces return the director to its rest configuration. In general, the electro-optical response of PDLC systems exhibits hysteresis, i.e. the transmittance measured with decreasing field is higher than the transmittance measured with increasing field (*9*). The basic reason for hysteresis in nematic droplet-dispersed polymer films has been the topic of several discussions, with suggestions that it might possibly be due to defect movement in a droplet (*10–12*), related to the mechanism of orientation of the droplet director (*13*) or result from a distribution of the LC droplet size and shape within the PDLC (*14*). Lacquet and co-workers (*7*) found that incomplete cured sensors showed hysteresis, whereas those that have been cured for an adequate time showed none or little effect.

Another interesting optical effect, the so-called memory effect, still remains a poorly understood aspect of PDLC electro-optical behavior. This effect refers to the existence in some systems (*5, 9, 15–17*) of

*Corresponding author. Email: madalena.dionisio@dq.fct.unl.pt

ISSN 0267-8292 print/ISSN 1366-5855 online

DOI: 10.1080/02678290801932850
http://www.informaworld.com

two distinct transparency states for zero applied electrical field: state 1, obtained after sample preparation or after heating it to the clearing temperature of the LC and after cooling, and state 2, which corresponds to a higher transparency in the OFF state reached after submitting the sample to an electric field above a critical value. This memory state is stable for a long period of several months at room temperature and can be erased by heating the cell to the clearing temperature of the LC. Some possible explanations given in the literature are mostly related with morphologic aspects where a more complex polymer ball structure lacking distinct LC droplets originates stronger memory effects (*5*, *9*, *17*). However, even in PDLC composites where LC exists in microdomains, the effect has also been observed and correlated with the anchoring property of LC molecules on polymer/LC interface walls (*9*, *17*).

In the present work we studied this effect on triethylene glycol dimethacrylate (TrEGDMA)/E7 composites using both electro-optical measurements and dielectric relaxation spectroscopy (DRS). DRS may provide useful information since it monitors the molecular mobility through the reorientation of molecular dipoles under the influence of a small oscillating electrical field. It also contributes to an understanding of the orientation of the LC director under an electrical field, which plays a major role in the PDLC performance and anchoring effect.

One of the main objectives of this work is to show that the memory effect detected in our systems is closely related to the loss or breakage of anchoring caused by the applied field. This anchoring breakage consists of the loss of surface-induced orientation of the LC molecules adjacent to the polymer wall above a critical field (E_c).

The chosen pre-polymer, TrEGDMA, is a dimethacrylate difunctional monomer, and the LC used is the nematic mixture E7, since a number of PDLC composites obtained from starting mixtures of acrylate-type monomers and E7 have revealed suitable electro-optical properties (*18–21*).

Among these polymer precursors, the influence of functionality on the electro-optical response has been evaluated (*22*), where higher fields are required to obtain a complete orientation of the director in the LC inclusions for PDLC composites produced from higher functional monomers due to the enhanced network density. In particular, the addition of a difunctional to a trifunctional diacrylate monomer lowers the field needed to attain a transparent state and increases the transmission in the ON state (*22*). The polymerisation of TrEGDMA monomer in the composite, generating the phase separation process, was thermally induced according to a free radical mechanism starting from an homogenous pre-polymer–LC mixture (*23*). The rate and extent of the polymerisation reaction, at which the phase separation sets in, strongly influence the LC domain shape and size (*24*) and, thus, the electro-optical response. To evaluate the influence of polymerization method, TrEGDMA/E7 mixtures with ratios equal to those prepared by thermal initiation that revealed better electro-optical response were also prepared by photochemical initiation.

2. Experimental

Materials

The nematic liquid crystalline mixture E7, with the composition (*25–27*): 4-cyano-4′-pentyl-1,1′-biphenyl (51%), 4-*n*-heptyl-4′-cyanobiphenyl (25%), 4,4′-n-octyloxycyanobiphenyl (16%) and 4′-*n*-pentyl-4-cyanoterphenyl (8%) w/w, was supplied by Merck kGaA (Darmstadt, Germany). The triethylene glycol dimethacrylate monomer, TrEGDMA, with M_w=286.36, was supplied by Fluka. The monomer was previously passed through a disposable inhibitor remover column from Aldrich in order to eliminate the hydroquinone stabilizer. The initiator for the thermal polymerisation was 2,2′-azobis(isobutyronitrile) (AIBN) from Aldrich, whereas 2,2-dimethoxy-2-phenylacetophenone (Irgacure 651) supplied by Ciba-Geigy was used as photoinitiator. Both initiators were used as received without further purification.

Preparation of PDLC samples

Monomer and E7 (TrEGDMA/E7) were mixed at room temperature until the mixture became homogeneous in the weight ratios 30:70, 40:60, 50:50 and 60:40. The mixtures also contain AIBN in the proportion 0.1% w/w relative to TrEGDMA as thermal initiator. The 30:70 and 40:60 mixtures were also prepared for photopolymerization using Irgacure 651 in the proportion of 1% w/w relative to TrEGDMA as photochemical initiator.

Samples were prepared by introducing via capillarity the mixtures into 20 μm thick ITO-coated glass LC cells (5 × 5 mm of ITO area) supplied by Instec, Inc, USA.

Thermal polymerisation was achieved isothermally by keeping the LC cells filled with the precursor mixtures in a sample holder (BDS 1200 from Novocontrol) 2.5 h at 70°C. The temperature control was assured by Quatro from Novocontrol. Photopolymerisation was accomplished by exposing the LC cells to UV radiation for 20 min through a light conducting fibre located 4.5 cm above the LC cell, to

ensure complete sample illumination, using a UV lamp from Hanovia. In order to avoid the heating effect of the photocuring source and to isolate the 365 nm wavelength, a solid heat filter (Schott, KG-1) and a 365 blue filter (SchottVG-9) were placed into the filter holder. All photopolymerisations were carried out at room temperature and with an incident light intensity of 2.33 mW cm^{-2}.

After the polymerisation process, the samples always looked opaque.

Electro-optical measurements

Electro-optical characterization was performed using a He–Ne (λ=633 nm) laser equipped optical bench fitted with a photodiode detector system and an ac controllable high-voltage generator for sample excitation. The samples were submitted to short bursts of 5 kHz ac voltage with 30 ms duration and a 1 s repetition rate for varying maximum amplitude while the transmission coefficient was recorded at each maximum amplitude. The voltage excitation scheme consisted of voltage sequences each one comprising an increasing step ramp up to a maximum value (V_{max}) followed by a decreasing step ramp down to the starting value (0 V).

This excitation method was used to better evidence the changes in the optical response detected in the samples associated with the anchoring breakage mechanism.

The complex capacitance of the samples was also recorded by measuring, besides the applied ac voltage, the ac electrical current going trough the cell.

The results reported were obtained for normal sample incidence at an ambient temperature of 20°C.

Scanning electron microscopy (SEM)

LC cells for SEM analysis were previously immersed in acetonitrile for a definite time in order to extract E7. Drying was accomplished by heating at 70°C under vacuum. To obtain an interface representative of the bulk morphology, the LC cell was fractured in liquid nitrogen. The resulting samples were mounted on aluminium stubs using carbon cement (D-400, Neubaeur Chemikalien) and a 3 ± 6 nm thick gold coating was deposited using a dual ion beam sputter coating apparatus. SEM images were obtained on a SEM Hitachi S2400 instrument with Rontec standard EDS detector.

Dielectric relaxation spectroscopy (DRS)

The dielectric measurements were carried out using a broadband impedance analyser, Alpha-N analyser from Novocontrol GmbH, covering a frequency range from 10^{-1} Hz to 1 MHz. The LC glass cell was placed between two gold-plated electrodes (diameter 20 mm) of a parallel plate capacitor and the electrical contact was assured by two copper wires. The sample cell (BDS 1200) was mounted on a cryostat (BDS 1100) and exposed to a heated gas stream being evaporated from a liquid nitrogen dewar. The temperature control was performed within ±0.5°C, with the Quatro Cryosystem. Novocontrol GmbH supplied all these modules.

Dielectric spectra were collected from -70 to 0°C in increasing temperature steps for samples before and after anchoring breakage. Additionally, to recover the initial anchoring state, a ramp experiment was performed at 10 K min^{-1} to a final temperature of 70°C, at fixed frequencies (10^5, 10^4, 10^3 and 10^2 Hz).

To achieve anchoring breakage, an ac voltage was applied to the LC sample cell within the dielectric sample holder, which was disconnected from the impedance analyser to prevent any damage. Thus, dielectric measurements were never performed under external voltage application. The ac voltage was obtained from a high-voltage TREK610C amplifier controlled by a low-voltage function generator. The frequency was set to 5 kHz, while the voltage application lasted for 3 min.

3. Results and discussion

PDLC electro-optical characterisation with pulsed voltage excitation

To obtain an initial insight into the electro-optical performance of the produced PDLC systems, the optical transmission was measured using the field sequence described above. Figure 1 shows the transmission vs. field curve obtained for the 30/70 TrEGDMA/E7 composite thermally polymerised (full circles). This composition shows an electro-optical response significantly improved relative to the remaining films in terms of the transmittance obtained in the ON and Off states and switching field ($E_{90\%}$=9.6 V μm^{-1}). The response of the respective 30:70 photopolymerised PDLC is also included in Figure 1 (open circles) exhibiting a significant higher switching field.

In order to relate the PDLC transmission–field response to the composite morphology, both 30:70 TrEGDMA/E7 systems were analysed by SEM. The respective SEM images are shown in Figure 2 for a) thermally and b) photo-prepared PDLCs.

Since E7 was removed prior to microscope analysis, the voids and dark areas in the micrographs are representative of the original E7 domains. At this

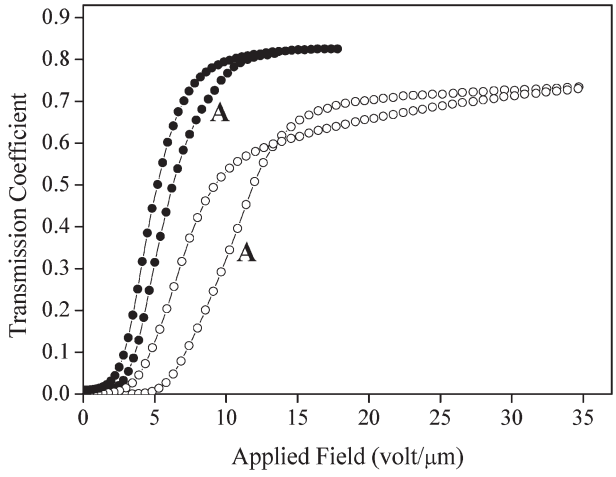

Figure 1. Field dependence of the transmission coefficient for both thermally (full circles) and photo- (open circles) polymerised mixtures of the 30:70 TrEGDMA/E7 PDLC. Both sets of data represent a complete cycle of incrementing the applied field up (up arrows) to a maximum value followed by a decrease down to zero (down arrows).

high E7 concentration, a two-phase morphology is observed where the LC phase seems to become quasi-continuous among a porous open cell structure formed by the polymerization of the monomer. The observed morphology is similar to the one found in pentacrylate/E7 systems (*28*) for LC concentrations of the order of 50%. At these concentrations there is insufficient monomer to fully construct a restrictive matrix and the LC phase condenses into a continuous phase (*28*). Because of the large composition of non-reactive component, E7, polymerisation of the monomer results in the formation of small polymer beads, which are insoluble in the LC, precipitating and phase separating out, aggregating to form a network structure. The SEM image for 30:70 photo-polymerised composite (Figure 2(b)) shows smaller and grainy polymer beads relatively to the thermally polymerized material with larger and smoother beads (Figure 2(a)). The inferior size of polymer globules in the photochemically polymerised composite can be an indication of higher cross-linking polymerisation leading to a higher network density. The remaining voids/dark areas in this composite are of smaller size relative to the thermally polymerised material indicating that LC domains in the photopolymerised PDLC are of inferior dimensions. This justifies the need for a higher field to achieve the transparent state in this material, in line with the inverse proportionality between LC size domain and switching field (*5*).

The electro-optical response of all the TrEGDMA/E7 composites studied exhibits anomalous hysteresis compared to other conventional

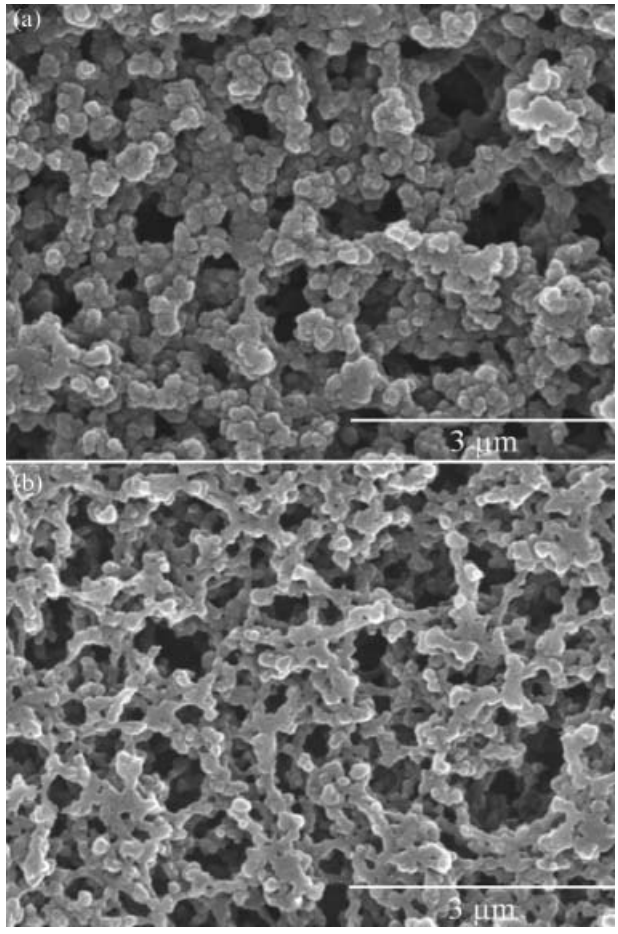

Figure 2. SEM images of the 30:70 TrEGDMA/E7 PDLC samples (a) thermally and (b) photopolymerised; E7 was removed previously so voids and dark areas are representative of the original LC domains that have lower dimensions in the photopolymerised composite (micrograph b).

systems (*7, 14, 29*), accompanied by an irreversible change in the transmittance for $0\,V\,\mu m^{-1}$ field. Whereas hysteresis is clearly seen in all the composites studied, the irreversible change in transmittance the OFF state shows better in the 40:60 system. To explore this feature in more detail, the composites were measured using field sequences starting from $0\,V\,\mu m^{-1}$ and reaching progressively higher maximal values (see section 2). Figure 3(a) illustrates the field dependence of the light transmittance for the 40:60 TrEGDMA/E7 thermally produced PDLC submitted to this type of stimulus.

Five field sequences with increasing E_{max} ranging from 6.5 to $27\,V\,\mu m^{-1}$ produced significantly different optical responses with and without hysteresis and memory effect. For $E_{max}=6.5\,V\,\mu m^{-1}$ no hysteresis occurs; see inset to Figure 3(a), where values measured in the increasing voltage step ramp (full squares) and decreasing voltage step ramp (open squares) are

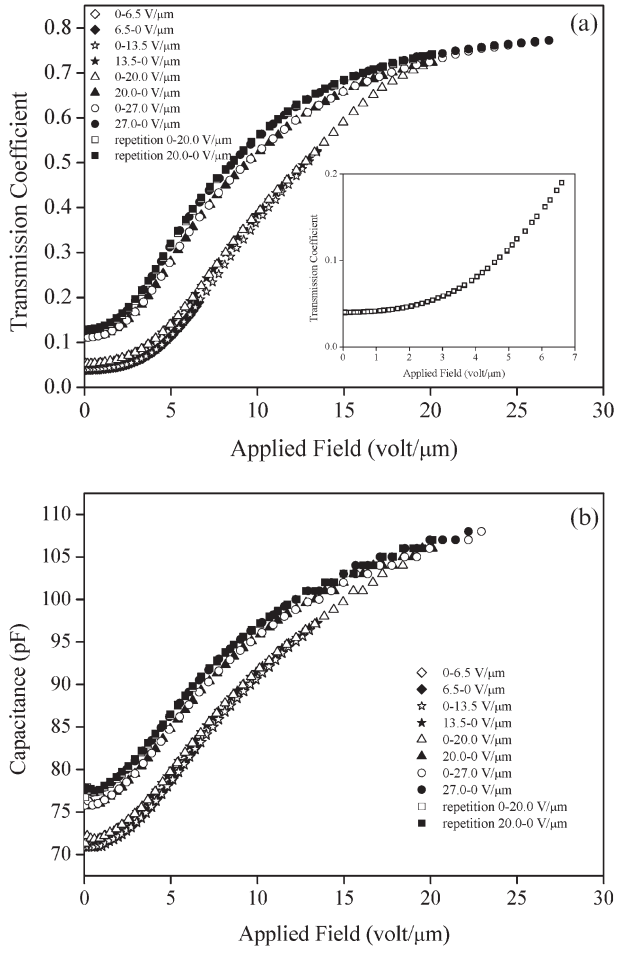

Figure 3. Field dependence of the (a) transmission coefficient and (b) capacitance for the 40:60 thermally prepared composite, following five sequence fields [only three representative field sequences are shown in (b)], illustrating both hysteresis and memory effects. The inset in (a) concerns the first field sequence (from 0 to 6.5 V μm^{-1}) where complete reversibility occurs.

completely superimposed. In the subsequent run up to 13.5 V μm^{-1}, a small hysteresis (full vs. open circles) but no memory effect is observed. In the following run, up to 20 V μm^{-1}, both hysteresis and memory effect become significant (full vs. open triangles) and the final transmission of the reverse scan in the absence of field is significantly higher relative to the initial transmission in the OFF state. Subsequent runs do not show relevant changes from the decreasing voltage step ramp with $E_{max}=20\,V\,\mu m^{-1}$. The discontinuity, observed in the transmittance in the OFF state after exceeding a critical field, was found for all the composites. The reverse scan only superimposes the forward scan at fields bellow that critical value.

A similar behaviour was found in the real capacitance of the sample estimated from ac current measurements obtained simultaneously with light transmission, presented in Figure 3 b, for the same 40:60 composite; only three representative field sequences are shown.

Table 1 summarises the electro-optical and capacitance data for the different composites.

The memory effect is evidenced by comparing $T_{(\sim 0V/\mu m)}$ and $C_{(\sim 0V/\mu m)}$ data measured before (BE_c) and after (AE_c) application of a critical field (E_c). Both light transmittance and capacitance are always higher after E_c has been applied. A decreasing tendency of E_c with increasing LC content can also be observed.

To understand the memory effect we can consider that the director field in LC-rich domains is determined by a balance between the elastic, the electrical and the interfacial contributions to the free energy of the nematic (*30*). In our system two different states corresponding to different director configurations without electrical field are observed; one, obtained after sample preparation or after heating it above the clearing point, and the other obtained after submitting the sample to a field above E_c. These two distinct configurations of the director field in the LC-rich domains at zero applied field must correspond to two different contributions of the elastic and interfacial parts to the total free energy of the nematic. This difference was promoted in a permanent fashion by a field above E_c. Considering the two contributions at play for the total free energy that could have been altered, the interfacial part of the free energy is the most likely to be changed through the occurrence of anchoring breakage.

Table 1. Electro-optical parameters of the samples studied, obtained with the pulsed excitation method. E_c is the critical field for anchoring breakage determined from the electro-optical data. BE_c and AE_c refer, respectively, to transmittance (T) and capacitance (C) values measured before and after the application of the critical field, E_c.

Polymerisation	TrEGDMA/E7 composition	$T_{(\sim 0\,V/\mu m)}$ (BE_c)	$T_{(\sim 0\,V/\mu m)}$ (AE_c)	T_{max}	E_c/V μm^{-1}	$C_{(\sim 0\,V/\mu m)}$/pF (BE_c)	$C_{(\sim 0\,V/\mu m)}$/pF (AE_c)	C_{max}/pF
Thermal	60/40	0.72	0.77	0.88	~15.0	62.6	65.6	79.4
	50/50	0.31	0.50	0.81	~9.5	68.1	74.6	95.0
	40/60	0.04	0.16	0.79	~11.3	70.7	78.9	111.1
	30/70	9.72E-04	0.015	0.83	~7.5	76.5	88.6	127.0
Photo	30/70	2.71E-04	0.0012	0.74	~12.5	76.3	81.5	127.3

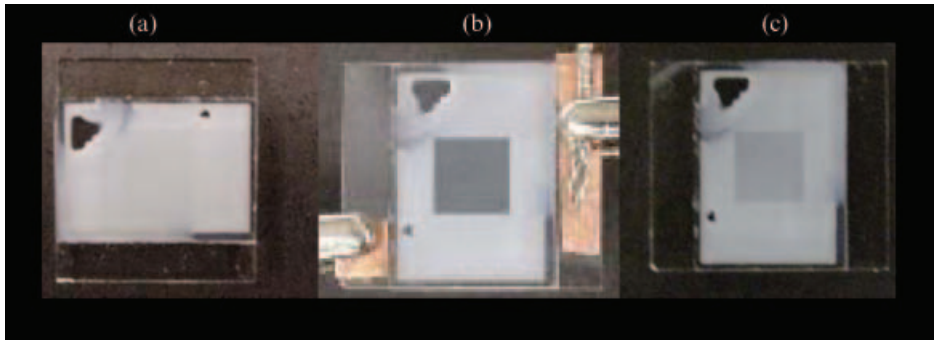

Figure 4. Images of the TrEGDMA/E7 40:60 thermally polymerized PDLC obtained: (a) initial OFF state, (b) upon applying tension and (c) OFF state after a critical field was exceeded.

Figure 4 compares the transparency in the absence of an applied voltage for the 40:60 composite before (Figure 4(a)) and after (Figure 4(c)) anchoring breakage; Figure 4(b) shows the transparency in the ON state.

The higher transparency obtained in the OFF state, after anchoring breakage is a permanent effect at room temperature; it is only possible to recover the initial opaque state if the sample is heated above the clearing point of E7 (60°C).

Dielectric relaxation spectroscopy

Bulk E7.

The nematic mixture E7 easily avoids crystallisation, entering a supercooled regime that upon further cooling vitrifies at a glass transition temperature around −60°C (*31, 32*). By studying E7 in the supercooled state, it was possible to bring into our frequency window (0.1 Hz–1 MHz), the relaxation processes usually observed in the nematic state in the megahertz and low gigahertz frequency regions. The complete dielectric characterisation is reported elsewhere for bulk E7 (*26, 27*) and for the 60:40 TrEGDMA/E7 composite (*33*).

Since liquid crystals are anisotropic systems, their dielectric properties are also anisotropic and the complex dielectric function $\varepsilon^*(\omega)$ (ω=angular frequency) has a tensorial nature. For uniaxial nematic phases this tensor has two main components $\varepsilon^*_{//}(\omega)$ and $\varepsilon^*_{\perp}(\omega)$ parallel and perpendicular to the nematic director, respectively. The theory of dielectric relaxation of LCs is outlined briefly in Demus *et al.* (*34*). A more refined discussion is also found in the literature (*35, 36*). Each mesogenic unit has two components of the molecular dipole vector that are oriented longitudinally and transverse to its long axis. The dielectric response is due to correlation functions of the polarisation fluctuations parallel and perpendicular to the nematic director. In that semi-microscopic treatment the measured dielectric function parallel $\varepsilon^*_{//}(\omega)$ and perpendicular $\varepsilon^*_{\perp}(\omega)$ to the director comprises different weighted sums of the four underlying relaxation modes depending on the macroscopic orientation of the sample. The relaxation mode with the lowest frequencies is due to rotational fluctuations of the molecule around its short axis, usually called the δ-process, determining mainly $\varepsilon^*_{//}(\omega)$. The other three relaxation modes (different tumbling of the molecules around their long axis) have nearly the same relaxation rate and form one broad relaxation, α-process, which is mostly related to $\varepsilon^*_{\perp}(\omega)$ being observed at higher frequencies than the $\varepsilon^*_{//}(\omega)$ related process. The relative intensities or dielectric strengths of one process relative to the other depend on the order parameter of the sample under investigation.

In unaligned state the dipole moment relaxes complementary between parallel and perpendicular alignments relative to the applied electrical field, presenting simultaneously the typical features found in oriented samples. In electric field-induced parallel or homeotropic alignment, the permittivity is measured parallel to the long axis of the molecules and therefore perpendicularly to the electrode surfaces, whereas in the electric field-induced perpendicular or planar condition the permittivity is measured perpendicular to the long axis of the molecules.

In the present work, a 20 µm thick glass LC cell was filled with pure E7 and the dielectric spectra collected between −70 and 0°C. Figure 5 shows the frequency dependence at −42°C of the dielectric loss, ε'', i.e. the imaginary part of the complex dielectric constant ($\varepsilon^*=\varepsilon'-i\varepsilon''$) (black line). At frequencies above 10^5 Hz, additional dielectric losses are observed due to the ITO coating (*37*). The equivalent spectrum collected for pure E7 inserted between gold-plated electrodes is included in Figure 5 for comparison (black line), together with different alignment states (grey lines).

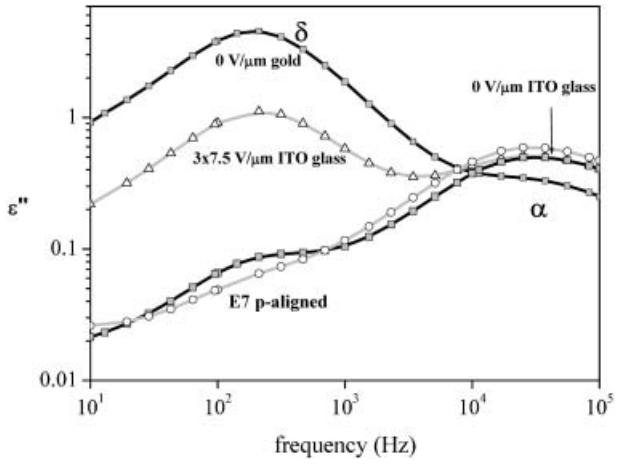

Figure 5. Dielectric relaxation spectra of pure E7 at −42°C inserted between gold plated electrodes ($0\,V\,\mu m^{-1}$ gold), ITO coated glass cells both in the initial state ($0\,V\,\mu m^{-1}$ ITO/glass) and upon applying tension (grey lines) evidencing the change in orientation of the liquid crystal; the planar alignment (p-aligned) was obtained after the application of a 7.5 V/μm field.

In bulk E7 lying between gold electrodes, the strongly predominant peak is related to the homeotropic alignment (ε''), δ-peak, whereas the high frequency flank mainly associated with planar alignment ($\varepsilon''_{\perp}$), α-peak, is of very low intensity (ε'' axis is in logarithmic scale). It is evident that the dramatic change in the alignment of the LC director when E7 is supported between two glass plates, as shown by the variation in the relative magnitudes of the dielectric strength, represent δ and α relaxation processes.

A further parameter obtainable from dielectric measurements is the LC director order parameter, S_d, that, according to Attard *et al.* (*38, 39*), can be computed from the observed complex permittivity and the respective ε^* values of the fully homeotropic and planar alignments; simple equations can be derived for either real or imaginary parts of ε^*. An alternative to the equation derived for S_d in terms of the real permittivity is proposed by Van Boxtel *et al.* (*40*), expressing S_d as a function of the dielectric strength that can be rewritten, for both α and δ-peaks, as:

$$\Delta\varepsilon_{\delta} = \left(\frac{\Delta\varepsilon_{\delta,//}}{3} + \frac{2\Delta\varepsilon_{\delta,\perp}}{3}\right) + \frac{2}{3}\left(\Delta\varepsilon_{\delta,//} - \Delta\varepsilon_{\delta,\perp}\right)S_d, \quad (1)$$

$$\Delta\varepsilon_{\alpha} = \left(\frac{\Delta\varepsilon_{\alpha,//}}{3} + \frac{2\Delta\varepsilon_{\alpha,\perp}}{3}\right) + \frac{2}{3}\left(\Delta\varepsilon_{\alpha,//} - \Delta\varepsilon_{\alpha,\perp}\right)S_d, \quad (2)$$

where $\Delta\varepsilon_i$ is the experimental dielectric strength of the i-peak and the // and $\perp$ subscripts indicate the dielectric strengths of, respectively, fully aligned parallel (homeotropic) and perpendicular (planar) conditions. Both Equations (1) and (2) should yield to the same value of the director, S_d, that, for a completely parallel-aligned LC takes the value of 1, whereas it is −0.5 for a completely perpendicularly aligned material; a null value is expected for a completely random state.

In order to apply these expressions to estimate S_d, we need also to estimate the relaxation strengths corresponding to the fully homeotropic and planar states. This was done through an optimisation process so that the $S_{d,i}$, $\Delta\varepsilon_{\delta,//}$, $\Delta\varepsilon_{\delta,\perp}$, $\Delta\varepsilon_{\alpha,//}$ and $\Delta\varepsilon_{\alpha,\perp}$ were those that minimise the differences between the modelled and experimental values of $\Delta\varepsilon_{\delta}$ and $\Delta\varepsilon_{\alpha}$, estimated from the Havriliak–Negami equation (*41*) obtained for bulk E7 in different aligned states; the remaining fit parameters are published elsewhere (*26*).

The S_d values corresponding to the dielectric spectra shown in Figure 5 are included in Figure 6 and presented in Table 2, together with values estimated for further aligned states. Values denoted as ($0\,V\,\mu m^{-1}$) represent measurements where no external field was applied, being clear that the alignments on gold and ITO/glass are very close to, respectively, fully homeotropic (S_d=0.99 on gold surface) and planar (S_d=−0.46 on ITO/glass) states. The almost fully perpendicular state was obtained after the application of a field of $7.5\,V\,\mu m^{-1}$, with no δ-peak, as can be observed in Figure 5 (denoted as E7 p-aligned). The director order parameter always takes negative values when E7 is supported between ITO/glass substrates for the applied fields. The obtained S_d values are in reasonable agreement with those reported earlier for a similar low temperature (−40°C) (*40*).

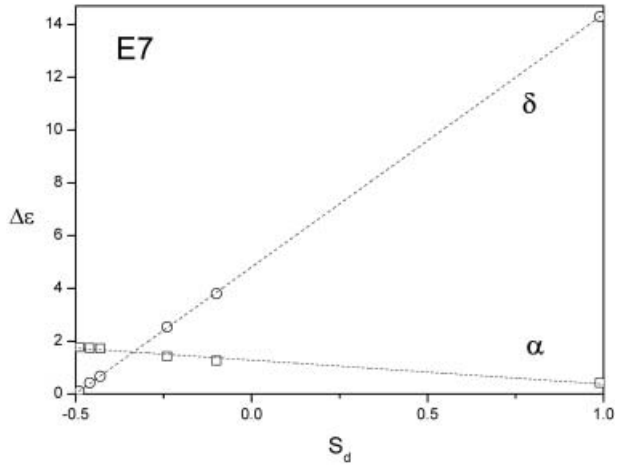

Figure 6. Linear dependence of the experimental dielectric strength, $\Delta\varepsilon$, with the director order parameter, S_d, for bulk E7, estimated according equation (1), denoted as δ, and Equation (2), denoted as α

Table 2. Director order parameter (S_d) and dielectric strengths ($\Delta\varepsilon$) from fits of the δ- and α-peaks estimated from equations (1) and (2) for different aligned states of bulk E7 inserted between gold and ITO/glass cells; $0\,V\,\mu m^{-1}$ represents the initial states where no field was applied. h- and p-aligned mean, respectively, fully homeotropic (//) and planar states ($\perp$).

Pure E7	$\Delta\varepsilon$ (δ)	$\Delta\varepsilon$ (α)	S_d
p-aligned	0.01	1.74	−0.50
h-aligned	14.4	0.41	1.00
$0\,V\,\mu m^{-1}$ gold	14.3	0.42	0.99
$0\,V\,\mu m^{-1}$ ITO glass	0.42	1.74	−0.46
$7.5\,V\,\mu m^{-1}$ ITO glass	0.103	1.77	−0.49
$2\times7.5\,V\,\mu m^{-1}$ ITO glass	0.67	1.73	−0.43
$3\times7.5\,V\,\mu m^{-1}$ ITO glass	2.54	1.43	−0.24
$4\times7.5\,V\,\mu m^{-1}$ ITO glass	3.8	1.26	−0.10

Since dielectric spectra of E7 inserted in gold and ITO/glass cells were obtained without application of any external electrical field, the observed orientational changes of the LC director depend on the interaction with the substrate and thus result from surface-induced alignment.

40:60 (TrEGDMA/E7) PDLC.

Given that the TrEGDMA/E7 40:60 composite originated the highest memory effect in both transmission and capacitance measurements, this composition ratio was chosen for further studies by dielectric relaxation spectroscopy between −70 and 0°C, in both thermally and photopolymerised PDLCs.

Figure 7 shows the dielectric loss spectrum of this composite at −42°C for thermally (squares) and photo- (triangles) polymerised PDLCs before (open symbols) and after (full symbols) anchoring breakage (achieved by applying $19.25\,V\,\mu m^{-1}$ at 5 kHz).

As a first observation, E7 presents a global alignment of the type found when inserted in non-glass material, which is an indication that E7 in the PDLC film is not in direct contact with the glass surface of the LC cell; thus, it is mainly encapsulated within the polymer matrix.

It must be pointed out that the dielectric response of the polymer film is not significant, as shown by the same profile of the loss peak obtained in the composite when compared with pure E7 [the temperature dependence (*33*) of ε'' at 1 and 100 kHz for both poly-TrEGDMA and the TrEGDMA/E7 composite in a different composition ratio, 60/40, demonstrate that the polymer has no meaningful dielectric response from −60°C up to 0°C in contrast with the PDLC response]. The relaxation spectra of the PDLC is of lower intensity compared with bulk LC, as expected for the dielectric response of an equivalent electrical circuit constituted by an association of two RC circuits, each one describing each bulk component, where the individual RC circuit for poly-TrEGDMA, have very low capacitance and high resistance.

From Figure 7, it is evident that after applying $19.25\,V\,\mu m^{-1}$ the δ-peak increases its height. This effect is more pronounced in the thermally polymerised sample. One should note, nevertheless, that the applied voltage in both transmission and capacitance measurements almost equals the value necessary to achieve a final transparent state in the

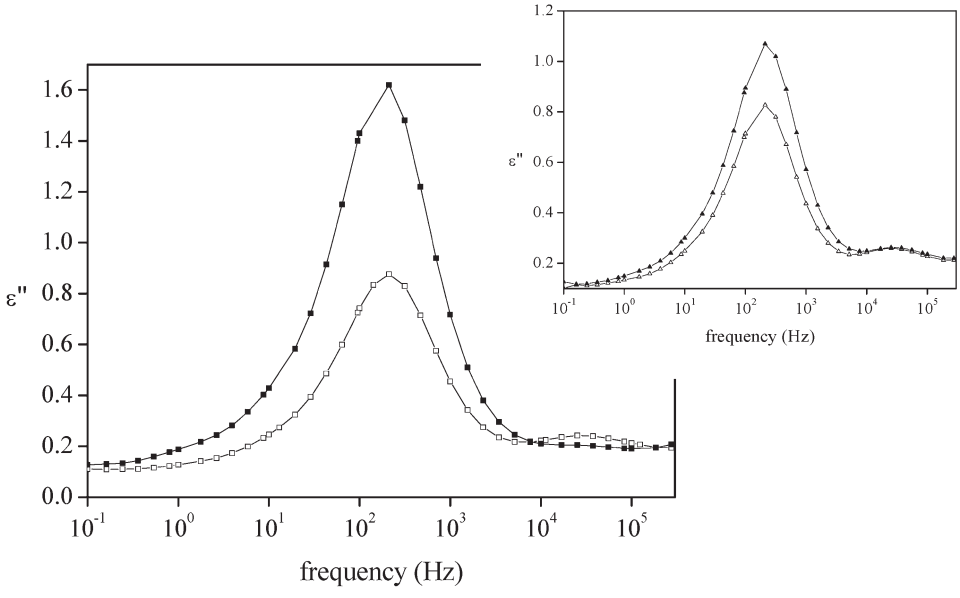

Figure 7. Dielectric relaxation spectra of TrEGDMA/E7 40:60 at −42°C before (open symbols) and after (full symbols) anchoring breakage by applying $19.25\,V\,\mu m^{-1}$ at 5 kHz, for thermal (squares) and photo- (triangles) polymerised composites.

thermally produced PDLC (see Figure 3(b)), whereas in the photopolymerised material, the applied field is insufficient to attain a saturation in any of those properties.

The temperature dependence of the dielectric loss at a fixed frequency, 1 kHz, is shown in Figure 8, taken from isothermal measurements after the application of different fields. It should be noted that in the temperature axis the detected processes are located in an opposite manner relative to that observed in the frequency axis; thus, the α-process is observed at lower temperatures relatively to the δ-peak.

It is evident that the δ-peak increases its height upon increasing the field. Once more, this effect is more pronounced in the thermally polymerized sample (main figure) comparing to the photopolymerised composite (right inset): full squares in both main figure and right inset show the temperature dependence of the dielectric loss after applying a field of $19.25\,\mathrm{V\,\mu m^{-1}}$.

To recover the initial state, the sample submitted to an increasing field was heated up to 70°C, i.e. above the LC clearing point (T_{NI}=60°C), followed by cooling to −80°C. After this, a ramp experiment was performed by increasing the temperature at a rate of $10\,\mathrm{K\,min^{-1}}$ from −80°C up to 0°C, measuring the dielectric loss at fixed frequencies, as shown in the left inset of Figure 8 for ε'' collected at 1 kHz (circles). It is evident that the sample has recovered the initial anchored state, as shown by the coincidence with the loss curve taken before any applied tension (squares); thus complete reversibility of E7 orientation exists if the clearing point is surpassed.

From the peaks intensity of the thermal prepared PDLC (main graph in Figure 8), the increase in the main δ peak was plotted as a function of the applied field (Figure 9). It can be clearly seen that the anchoring breakage occurs in the field amplitude range from 15 to $20\,\mathrm{V\,\mu m^{-1}}$, whereas at fields above this range no more anchoring breakage takes place. The inset to Figure 9 shows a plot of the decrease in the α-peak, also obtained from Figure 8. This decrease shows a symmetrical behaviour relative to that of the δ-peak. However their magnitudes do not

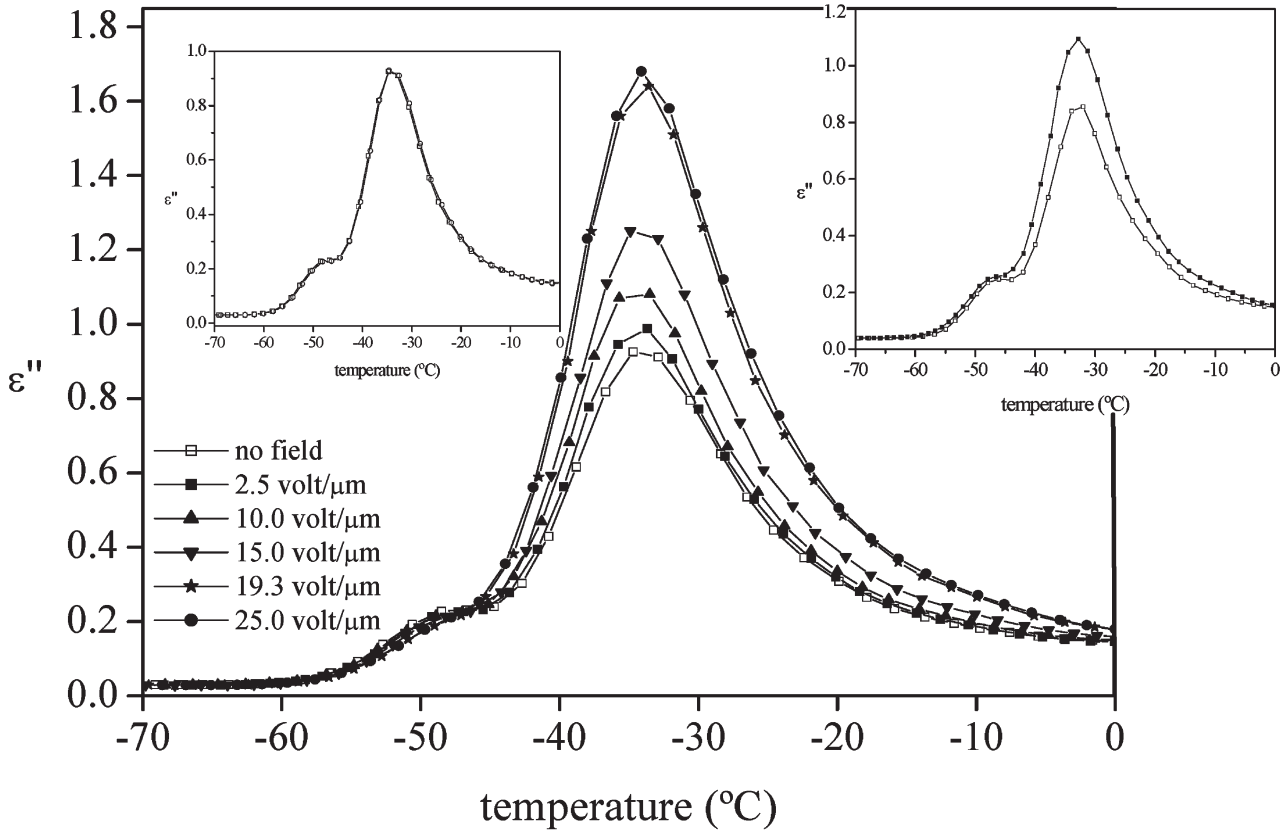

Figure 8. Temperature dependence of the dielectric loss at 1 kHz taken from isothermal measurements for TrEGDMA/E7 40:60 thermally prepared before (open symbols) and upon increasing field; right inset presents the same dependence for the correspondent photopolymerised composite where full symbols represent measurements obtained after applying $19.25\,\mathrm{V\,\mu m^{-1}}$. Left inset shows the complete superposition of the dielectric losses at 1 kHz, between measurements taken after application of $25\,\mathrm{V\,\mu m^{-1}}$ followed by heating at 70°C (circles) and before any applied tension (squares), evidencing total reversibility of E7 orientation, if its clearing point is surpassed.

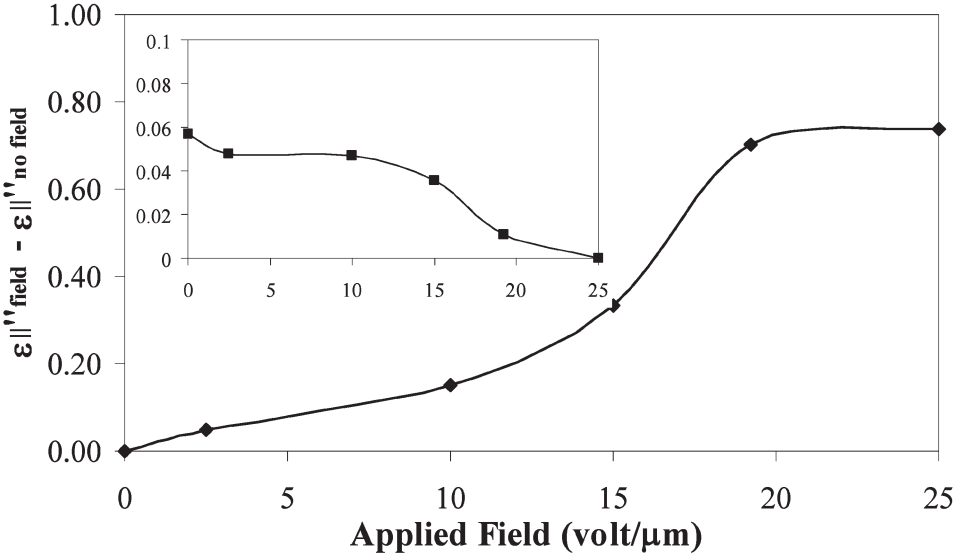

Figure 9. Field dependence of the variation of the dielectric loss at 1 kHz after different amplitude fields had been applied relative to the initial state (no field) measured at the temperature where the maximum of the δ-peak occurs ($T=-33.5^{\circ}$C, for ε'' 1 kHz), showing that the anchoring breakage occurs in the field amplitude range from 15 to 20 V μm^{-1}; the inset shows the concomitant decrease of the α-peak measured at -48.5°C, for ε'' 1 kHz. Variation calculated from data presented in Figure 8.

compensate each other, the δ-peak being much more significant.

Furthermore, the dielectric strengths of the isothermal peaks at -42°C, under the various experimental conditions presented in Figure 8, were used to calculate S_d through Equations (1) and (2). In this case, given that the dielectric strength values corresponding to the full aligned conditions in bulk E7 cannot be used to estimated S_d values in PDLC, since significant changes in magnitude occur as already commented, and because experimentally no fully aligned condition was achieved, a reasonable estimate of $\Delta\varepsilon_{\delta,//}$, $\Delta_{\varepsilon\delta,\perp}$, $\Delta\varepsilon_{\alpha,//}$ and $\Delta\varepsilon_{\alpha,\perp}$ starting values was not easy. In order to bypass this difficulty, capacitance (C) values presented in Figure 3(b) were used in equations analogous to Equations (1) and (2) but with ε' replacing $\Delta\varepsilon$, as first proposed by Attard and Williams (*38*); $\varepsilon'=C/C_0$, where C_0 is a geometrical capacitance. Two assumptions were made: (i) the capacitance measured at 22.5 V μm^{-1} corresponds to a fully homeotropic alignment, and (ii) $\varepsilon'_{//}+\varepsilon'_{\perp}\approx\varepsilon'_{//}$, which simplifies equation (1) to:

$$\frac{C_{AVc,\,0\,\mathrm{V}\,\mu\mathrm{m}^{-1}}}{C_0}=\frac{1}{3}\frac{C_{22.5\,\mathrm{V}\,\mu\mathrm{m}^{-1}}}{C_0}(1+2S_d), \qquad (3)$$

giving an estimate of 0.59 for S_d in the PDLC after anchoring breakage in the OFF state.

Final estimated values for the different aligned states presented in Figure 8 are presented in Table 3 and plotted in Figure 10.

It is evident that the increase in the S_d value is due to the increase of the height of the δ-peak; thus, upon application of the external field the sample aligns with the nematic director more parallel with the applied electrical field until saturation.

The observed effects could be interpreted by conceptualizing the LC domain as consisting of an interfacial shell of immobilized molecules due to the anchoring interaction with the polymer surface where the molecular long axis of LC is lying parallel to the surface. This interfacial shell holds in its interior bulk like molecules. The anchored molecules will influence the orientation of the adjacent ones through the elastic restoring forces arising in the deformed nematic. Before applying any field the director of

Table 3. Director order parameter (S_d) and dielectric strengths ($\Delta\varepsilon$) from fits of the δ- and α-peaks estimated from equations (1) and (2) for different applied fields in 40:60 TrEGDMA/E7 PDLC inserted between ITO/glass cells; h- and p-aligned mean, respectively, fully homeotropic (//) and planar states ($\perp$).

PDLC		$\Delta\varepsilon$ (δ)	$\Delta\varepsilon$ (α)	S_d
	p-aligned	0.06	0.88	−0.50
	h-aligned	5.40	0.4	1.00
Thermal	0 V μm^{-1}	2.073	0.67	0.07
	10.0 V μm^{-1}	2.34	0.67	0.14
	15.0 V μm^{-1}	2.62	0.70	0.22
	19.3 V μm^{-1}	3.76	0.541	0.54
	25.0 V μm^{-1}	3.81	0.53	0.55
Photo	0 V μm^{-1}	2.01	0.67	0.05
	25.0 V μm^{-1}	2.60	0.66	0.21

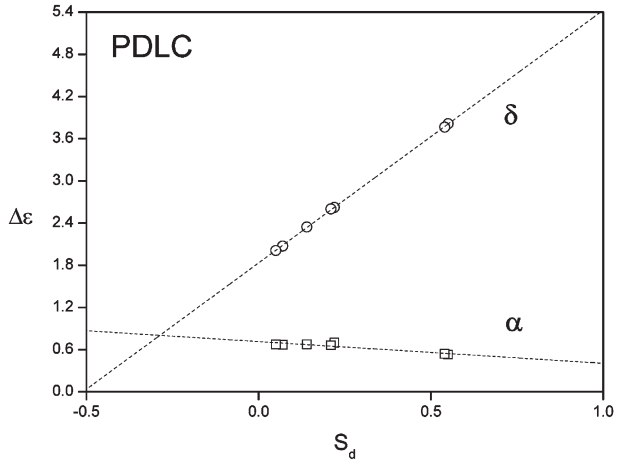

Figure 10. Linear dependence of the experimental dielectric strength, $\Delta\varepsilon$, with the director order parameter, S_d, for 40:60 TrEGDMA/E7 PDLC, estimated according Equation (1), denoted as δ, and Equation (2), denoted as α.

the LC inclusions is randomly distributed. Under the action of a field bellow E_c, the molecules in the bulk reorient along the field but the molecules anchored at the interface, impair a full homeotropic alignment (see Scheme 1(a)).

Above E_c, the anchoring of the molecules to the polymeric surface is broken and the molecules at the surface adopt an alignment towards the field direction that tends to persist after field removal. This alignment at the surface determines the orientation of the remaining LC giving rise to a higher transparency even in the OFF state (see Scheme 1(b)). Concomitantly to this higher transmission in the OFF state, a shift to lower values of the threshold field is observed (see Figures 1 and 3). The reduction of the threshold field upon addition of a second phase to a LC was described earlier for anisotropic thermoreversible gels in twisted nematic cells (*42*), and E7 confined within a colloidal network (*40*).

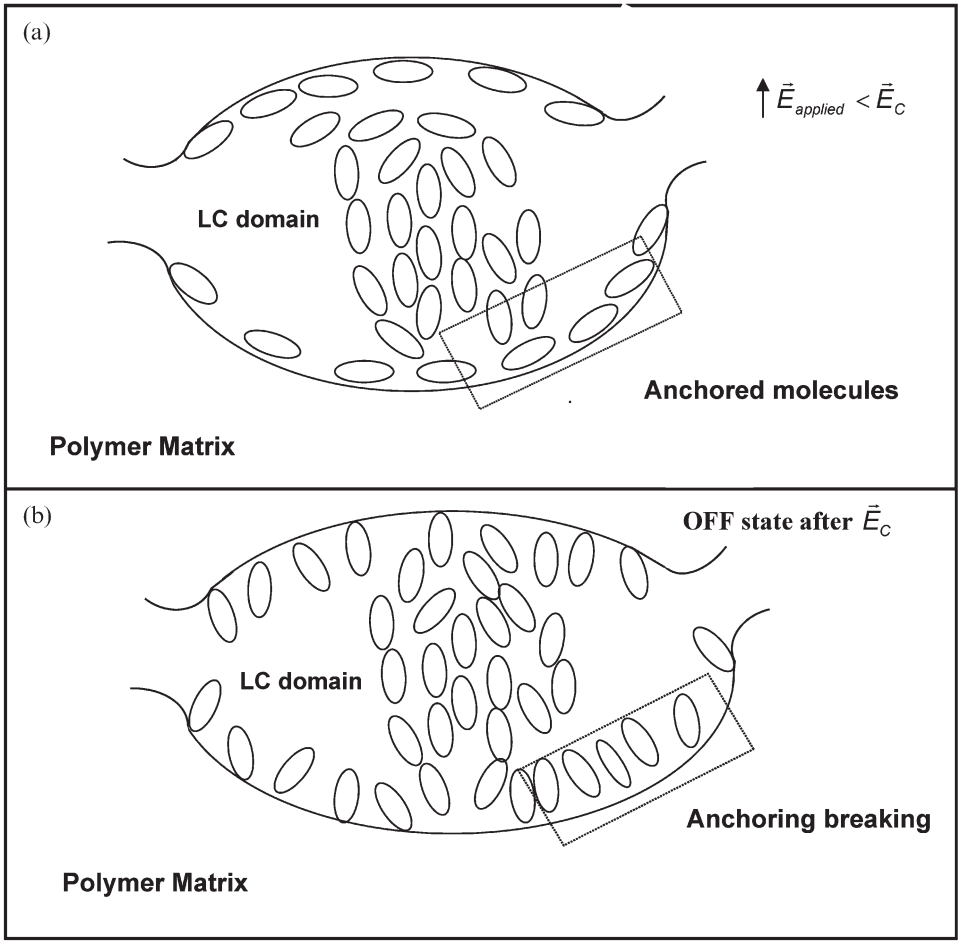

Scheme 1. Schematic drawing of the possible alignment of E7 molecules within the polymer matrix illustrating a) the E7 molecules anchoring to the polymer surface impairing a full homeotropic alignment when the applied electric field is below the critical value and b) the anchoring breaking of E7 molecules that adopt an alignment towards the field direction which tends to persist after the application of a field exceeding the critical value.

After the anchoring breakage caused by the high electric field, molecules align more readily with the applied field, i.e. the elastic energy needed to be overcome by the electric field is reduced.

Dielectrically, the memory effect manifests by an increase of δ loss peak mainly associated with the parallel alignment of the nematic director to the field.

Comparing the magnitude of the irreversible anchoring breaking effect in thermally and photopolymerised composites we observe that it is higher in the former, due to either bigger LC domains and/or a lower microscopic interaction between the LC and the polymer interface. Thus, in photopolymerised PDLC the smaller LC domains are more influenced by the polymer wall, which also explains the need for a higher voltage to overcome elastic deformation. This manifests in a lower degree of homeotropic orientation after applying the field (S_d in Table 3 equal to 0.21 against 0.55 in thermal PDLC).

After anchoring breakage, it is possible to recover the initial transparency in the OFF state if the sample is heated above the LC clearing point. Above T_{NI}, since the director field is not defined, the memory state is erased. On cooling, the director field is going to be set by the interplay of the surface interactions and the elastic energy, as happens in the newly prepared material.

4. Conclusions

Four different composition ratios (30:70, 40:60, 50:50 and 60:40) of TrGDMA/E7 mixtures were thermally polymerised and their dielectric and electro-optical properties evaluated. An irreversible effect occurs when the applied electric field exceeds a critical value resulting, macroscopically, in a higher transparency in the OFF state and a reduced threshold voltage in all our samples. This was rationalised in terms of an electric field driven anchoring transition and was studied by transmittance, capacitance and dielectric spectroscopy measurements. Dielectrically, the anchoring breaking reflects mainly by an increase in the δ peak. The LC orientation was probed by dielectric relaxation data exhibiting α and δ peaks. The director order parameter, S_d, estimated from the relative magnitude of the dielectric strengths of both detected processes, yielded a value at zero field that jumps from 0.07 before anchoring breakage to 0.55 after anchoring breakage in the thermally prepared composite with 40:60 poly-TrEGDMA/E7 ratio. In the PDLC, the LC always exhibited positive S_d values, whereas it shows negative values when in direct contact with ITO–glass surfaces. This indicates that the LC is mainly encapsulated in the polymer matrix.

Concerning the electro-optical response, the best performance was found for the 30:70 thermally prepared composite. The corresponding photopolymerised mixture revealed an inferior electro-optical behaviour, requiring superior fields to switch to the transparent state. This may arise from smaller liquid crystalline domains, as shown by SEM micrographs.

Acknowledgments

Financial support was provided by Fundação para a Ciência e Tecnologia (FCT) through the projects POCTI/CTM/37435/2001, POCTI/CTM/47363/2002 and FEDER. M. T. Viciosa acknowledges to FCT the PhD grant SFRH/BD/6661/2001.

References

(1) Crawford G.P., Žumer S. (Eds), *Liquid Crystals in Complex Geometries*; Taylor and Francis: London, 1996.
(2) Kitzerow H.S. *Liq.Cryst.* **1994**, *16*, 1–31.
(3) Schadt M. Annu. *Rev. Mater. Sci.* **1997**, *27*, 305–379.
(4) Doane J.W., In *Liquid Crystals – Applications and Uses*; Bahadur B. (Ed.), World Scientific: Singapore, 1990. pp. 361–395.
(5) Drzaic P.S. *Liquid Crystals Dispersions*; World Scientific: Singapore, 1995.
(6) Wu S.T., Yang D.K. (Eds), *Reflective Liquid Crystal Displays*; Wiley: New York, 2001.
(7) Lacquet B.M.; Swart P.L.; Spammer S.J. *IEEE Trans. Instrum. Meas.* **1997**, *46*, 31–35.
(8) Zhou J.; Collard D.M.; Park J.O.; Srinivasarao M. *J. Am. chem. Soc.* **2002**, *124*, 9980–9981.
(9) Han J. *J. Korean Phys. Soc.* **2006**, *49*, 1482–1487.
(10) Reamey R.H.; Montoya W.; Wong A. *Proc. SPIE* **1992**, *1665*, 2–7.
(11) Jain S.C.; Rout D.K. *J. appl. Phys.* **1991**, *70*, 6988–6992.
(12) Drzaic P.S. *Liq. Cryst.* **1988**, *3*, 1543–1559.
(13) Kelly J.R.; Palffy-Muhoray P. *Mol. Cryst. liq. Cryst.* **1994**, *243*, 11–29.
(14) Li Z.; Nelly J.R.; Palffy-Muhoray P.; Rosenblatt C. *Appl. Phys. Lett.* **1992**, *60*, 3132–3134.
(15) Yamagishi F.G.; Miller L.J.; van Ast C.I. *Proc. SPIE* **1989**, *1080*, 24.
(16) Yamaguchi R.; Sato S. *Jap. J. appl. Phys.* **1991**, *30*, 616–618.
(17) Han J. *J. Korean Phys. Soc.* **2003**, *43*, 45–50.
(18) Roussel F.; Buisine J.; Maschke U.; Coqueret X. *Mol. Cryst. liq. Cryst.* **1997**, *299*, 321–328.
(19) Roussel F.; Buisine J.; Maschke U.; Coqueret X.; Benmouna F. *Phys. Rev. E* **2000**, *62*, 2310–2316.
(20) Carbonnier B.; Best A.; Pakula T.; Benmouna M.; Maschke U. *Mol. Cryst. liq. Cryst.* **2004**, *409*, 183–189.
(21) Roussel F.; Maschke U.; Buisine J.; Coqueret X.; Benmouna M. *Phys. Rev. E* **2002**, *65*, 011706(1–8).
(22) Maschke U.; Coqueret X.; Benmouna M. *Macromol. Rapid Commun.* **2002**, *23*, 159–170.
(23) Pogue R.T.; Natarajan L.V.; Siwecki S.A.; Tondiglia V.P.; Sutherland R.L.; Bunning T.J. *Polymer* **2000**, *41*, 733–741.

(24) Kloosterboer J.G.; Serbutoviez C.; Touwslager F.J. *Polymer* **1996**, *37*, 5937–5942.
(25) Brás A.R.E.; Henriques S.; Casimiro T.; Aguiar Ricardo A.; Sotomayor J.; Caldeira J.; Santos C.; Dionísio M. *Liq. Cryst.* **2007**, *34*, 591–597.
(26) Viciosa M.T.; Nunes A.M.; Fernandes A.; Almeida P.L.; Godinho M.H.; Dionisio M. *Liq. Cryst.* **2002**, *29*, 429–441.
(27) Brás A.R.E.; Dionísio M.; Huth H.; Schick C.; Schönhals A. *Phys. Rev. E* **2007**, *75*, 061708(1–8).
(28) Vaia R.A.; Tomlin D.W.; Schulte M.D.; Bunning T.J. Polymer **2001**, *42*, 1055–1065.
(29) Van Boxtel M.C.W.; Wübbenhorst M.; Van Turnhout J.; Bastiaansen C.W.M.; Broer D.J. *Liq. Cryst.* **2004**, *31*, 1207–1218.
(30) Prost J.; De Gennes *The Physics of Liquid Crystals*; Oxford University Press: Oxford, 1992.
(31) Zhong Z.Z.; Schuele D.E.; Gordon W.L.; Adamic K.J.; Akins R.B. *J. Polym. Sci. B* **1992**, *30*, 1443–1449.
(32) Roussel F.; Buisine J.M.; Mascchke U.; Coqueret X. *Liq. Cryst.* **1998**, *24*, 555–561.
(33) Brás A.R.E.; Viciosa M.T.; Rodrigues C.M.; Dias C.J.; Dionísio M. *Phys. Rev. E* **2006**, *73*, 061709(1–11).
(34) Demus D., Goodby J., Gray G.W., Spiess H.W., Vill V. (Eds), *Handbook of Liquid Crystals*; Wiley-VCH: Weinheim, 1998.
(35) Nordio P.L.; Rigatti G.; Serge U. *Mol. Phys.* **1973**, *25*, 129–186.
(36) Williams G., In *The Molecular Dynamics of Liquid Crystals*; Luckhurst G.R., Veracini C.A. (Eds), Kluwer Academic: 1994. pp. 431–450.
(37) Fournier J.; Williams G.; Holmes P.A. *Macromolecules* **1997**, *30*, 2042–2051.
(38) Attard G.S.; Williams G. *Liq. Cryst.* **1986**, *1*, 253–269.
(39) Attard G.S.; Araki K.; Williams G. *Br. Polym. J.* **1987**, *19*, 119–127.
(40) Van Boxtel M.C.W.; Wübbenhorst M.; Van Turnhout J.; Bastiaansen C.W.M.; Broer D.J. *Liq. Cryst.* **2003**, *30*, 235–249.
(41) Havriliak S.; Negami S. *Polymer* **1967**, *8*, 161–210.
(42) Mizoshita N.; Hanabusa K.; Kato T. *Displays* **2001**, *22*, 33–37.